PCCP

PAPER

View Article Online
View Journal | View Issue

Published on 07 December 2015. Downloaded by Michigan State University on 22/01/2016 03:37:24.

Cite this: *Phys. Chem. Chem. Phys.*, 2016, **18**, 1945

Influence of gold species ($AuCl_4^-$ and $AuCl_2^-$) on self-assembly of PS-*b*-P2VP in solutions and morphology of composite thin films fabricated at the air/liquid interfaces†

Xingjuan Zhao,[a] Qian Wang,[a] Xiaokai Zhang,[b] Yong-Ill Lee[c] and Hong-Guo Liu*[a]

Received 16th October 2015,
Accepted 4th December 2015

DOI: 10.1039/c5cp06267e

www.rsc.org/pccp

Composite thin films doped with Au species were fabricated at an air/liquid interface *via* a series of steps, including the mass transfer of polystyrene-*b*-poly(2-vinylpyridine) (PS-*b*-P2VP) across the liquid/liquid interface between a DMF/$CHCl_3$ solution and an aqueous solution containing either $AuCl_4^-$ or $AuCl_2^-$, self-assembly of PS-*b*-P2VP in a mixed DMF–water solution, and adsorption and further self-organization of the formed aggregates at the air/liquid interface. This is a new approach for fabricating composite polymer films and can be completed within a very short time. $AuCl_4^-$ and $AuCl_2^-$ ions were found to significantly influence the self-assembly behavior of the block copolymer and the morphologies of the composite films, leading to the formation of nanowire arrays and a foam structure at the air/liquid interface, respectively, which originated from rod-like micelles and microcapsules that had formed in the respective solutions. The effect of the metal complex was analyzed based on the packing parameters of the amphiphilic polymer molecules in different microenvironments and the interactions between the pyridine groups and the metal chloride anions. In addition, these composite thin films exhibited stable and durable performance as heterogeneous catalysts for the hydrogenation of nitroaromatics in aqueous solutions.

Introduction

Amphiphilic block copolymers self-assemble into various micro and nanostructures. They can form a wide variety of ordered molecular assemblies in solutions including spherical, cylindrical, disk-like and lamellar micelles, vesicles, among many other aggregates.[1–5] Spin-coated or dip-coated films[6–10] with various microstructures have been fabricated by micellization and microphase separation of block copolymers.

The Langmuir monolayer technique is a useful method for fabricating low-dimensional supramolecular assemblies and ultrathin films at an air/liquid interface. The self-organization behavior of block copolymers, such as the amphiphilic PS-*b*-P4VP,[11] PS-*b*-PEO,[12,13] and conjugated PI-*b*-P3HT,[14] at the air/liquid interface has been investigated in recent years. PS-*b*-P2VP is an amphiphilic block copolymer. Its self-assembly behavior both in solutions and at the air/liquid interface has been widely investigated and various nanostructures including planar, rod-like, circular and necklace-network structures and nanowires have been fabricated.[15] The effects of the pH of the subphase[16,17] and the spreading solvents[18] on the self-organization of PS-*b*-P2VP and the formed nanostructures have been studied. Researchers have also fabricated composite nanostructures of PS-*b*-P2VP with other homopolymers[19,20] and block copolymers.[17,21] Interestingly, the temperature-triggered micellization behavior of PS-*b*-P2VP on the surface of an ionic liquid has been reported.[22]

Recently, the planar liquid/liquid interface formed by two immiscible liquids has also been utilized to fabricate polymer-based composite structures[23–26] due to its unique properties, which differ from those of the bulk phase and the air/liquid interface. Although the spreading behavior of PS-*b*-PEO at a cyclohexane/water interface was investigated as early as 1999,[27] the self-assembly behavior of block copolymers at the liquid/liquid interface has aroused considerable interest in recent years. For example, Taboada *et al.* analyzed the interface properties of poly(styrene oxide)-*b*-poly(ethylene oxide) at a chloroform/water interface,[28] Xu *et al.* studied the aggregation behavior of block polyethers at an *n*-heptane/water interface,[29] and Plamper *et al.*[30] investigated the interface-enforced complexation behavior between copolymer blocks at the oil/water (O/W) interface. Very interestingly, with the aid of the adsorption of

[a] *Key Laboratory for Colloid and Interface Chemistry of Education Ministry, Shandong University, Jinan 250100, P. R. China. E-mail: hgliu@sdu.edu.cn*
[b] *College of Physics and Electronics, Shandong Normal University, Jinan 250014, P. R. China*
[c] *Anastro Laboratory, Department of Chemistry, Changwon National University, Changwon 641-773, Korea*

† Electronic supplementary information (ESI) available. See DOI: 10.1039/c5cp06267e

Published on 07 December 2015. Downloaded by Michigan State University on 22/01/2016 03:37:24.

amphiphilic block copolymers and interactions between the polymers and water-soluble species, functional composite thin films have been fabricated at O/W interfaces. For example, Russell *et al.*[31] obtained PS-*b*-P2VP/graphene oxide composite films, He *et al.*[32] fabricated SERS-active conjugated block copolymer/Au nanoparticle composite films, and Du *et al.* fabricated monolayer thin films of $(P4VP–PS–P4VP)_n$-capped Au nanoparticles at the $(DMF–H_2O)$/diethyl ether interface.[33]

Recently, we found that amphiphilic block copolymers formed composite thin films with a variety of morphologies at the liquid/liquid interfaces between chloroform solutions of the polymers and aqueous solutions of inorganic species, such as $AgNO_3$ and $HAuCl_4$, through a process of adsorption and self-assembly.[34–38] The structure of the film can be tuned by changing the molecular structure of the polymers, nature of the inorganic species, and concentrations of the polymers and inorganic species. Shortly afterwards, to fabricate microstructures of block copolymers with strongly polar blocks, such as polystyrene-*b*-poly(acrylic acid)–polystyrene, a new method of emulsion-templated assembly and liquid/liquid interfacial adsorption was developed using a mixed solution of a polymer in DMF/chloroform as the oil phase to fabricate composite films.[39–41] The DMF migrated to the aqueous phase, while the water migrated across the interface to the organic phase as soon as the interface was formed, which resulted in the formation of W/O emulsions in the original organic solution due to the "ouzo effect".[42] The polymer molecules assembled around the droplets of the emulsion and coordinated with metal ions to form microcapsules, which further assembled into composite thin films that consisted of a foam structure doped with metal ions at the planar liquid/liquid interface.

Very recently, we attempted to fabricate composite structures of PS-*b*-P2VP with Ag^+ at the liquid/liquid interface using the emulsion-templated assembly method described above.[43] A mixed DMF/chloroform solution of the polymer and an aqueous solution of $AgNO_3$ were used as the organic and aqueous phases, respectively. Surprisingly, we found that a thin free-standing film appeared at the air/liquid interface rather than at the liquid/liquid interface. This interesting phenomenon was related to the transfer of PS-*b*-P2VP from the organic to the aqueous phase across the liquid/liquid interface along with DMF, self-organization of the polymer molecules with Ag^+ ions in the mixed water/DMF solution, adsorption, and further assembly of the generated organized molecular assemblies at the air/liquid interface. This is a new method for the fabrication of thin films at the air/liquid interface, which is based on the adsorption of organized molecular assemblies formed in solutions, and is quite different from the traditional Langmuir monolayer technique[11–21] and also from the traditional Gibbs adsorption of amphiphiles at the air/water interface. This study marks the further development of the interfacial assembly method of composite structures of block copolymers. Interestingly, the structure of the films depends on the molecular structure and other experimental parameters such as the concentrations of the polymer and Ag^+ ions, the volume ratios of DMF/chloroform, and the volume ratios between the organic and aqueous solutions. Shortly afterwards, a composite PB-*b*-P4VP multilayered film doped with Au nanoparticles was fabricated using the same method.[44]

In the study presented in this paper, we further fabricated composite films of PS-*b*-P2VP with gold species using the abovementioned method. Two types of aqueous solutions containing $HAuCl_4$ and $HAuCl_2$ were used. We found that composite films appeared at the air/liquid interfaces. Under certain conditions, the films formed a distinct structure, *i.e.*, parallel nanowires and a foam structure when using aqueous solutions of $AuCl_4^-$ and $AuCl_2^-$, respectively. The influences of several experimental parameters, such as the type of inorganic species, concentration of the polymer and the inorganic species, volume ratio of DMF and $CHCl_3$ in the organic solutions, and volume ratio of the organic solution and the aqueous solution, on the film structure were investigated. The formation mechanism was also discussed, and the catalytic activities of these composite structures were evaluated.

Experimental section

Materials

The block copolymer PS-*b*-P2VP with M_n values of 110 000/12 500 for the PS and P2VP blocks (Production No. P8721-*b*-S2VP; M_w/M_n = 1.09) was purchased from Polymer Source (Canada) and used as received. DMF ($\geq$99.5%) was obtained from Sinopharm Chemical Reagent Co. Ltd (Shanghai, China) and used as received. Chloroform (analytical reagent) containing 0.3–1.0% ethanol as a stabilizer was obtained from Guangcheng Chem. Co. (Tianjin, China). The water used was highly purified using a UP water purification system (UPHW-IV-90T, Chengdu, China) with a resistivity of $\geq$18.0 MΩ cm. KBH_4 ($\geq$97.0%) and $HAuCl_4{\cdot}3H_2O$ (99.9%) were purchased from Zhanyun Chem. Co. Ltd (Tianjin, China) and Aldrich, respectively. L-Ascorbic acid (99.7%) was purchased from Kermel Chem. Co. Ltd (Tianjin, China) and 4-nitroaniline (4-NA, $\geq$99.5%) was supplied by Tianjin Kemiou Chem. Reagent Co. Ltd.

Reduction of aqueous solution of $HAuCl_4$

About 10 μL of a freshly prepared 0.5 mol L^{-1} aqueous solution of ascorbic acid was added dropwise by a microsyringe into 5 mL aqueous solution of $HAuCl_4$ with a concentration of 0.001 mol L^{-1} with stirring using an electromagnetic stirrer. The resulting solution gradually changed from yellow to colorless, which indicated the reduction of Au(III) to Au(I) species.[45,46] The reduction process was monitored using UV-vis spectroscopy. As shown in Fig. 1, the absorption peak at 320 nm, which corresponds to $AuCl_4^-$, almost disappeared and no absorption peak corresponding to the surface plasmon resonance of Au nanoparticles appeared; this indicated that the $AuCl_4^-$ ions were reduced to $AuCl_2^-$ ions completely without further reduction.

Fabrication of the film at the air/liquid interface

Scheme 1 shows the fabrication process of the composite thin films. In a typical experiment, a 5 mL aliquot of a DMF/$CHCl_3$

 This journal is © the Owner Societies 2016

Published on 07 December 2015. Downloaded by Michigan State University on 22/01/2016 03:37:24.

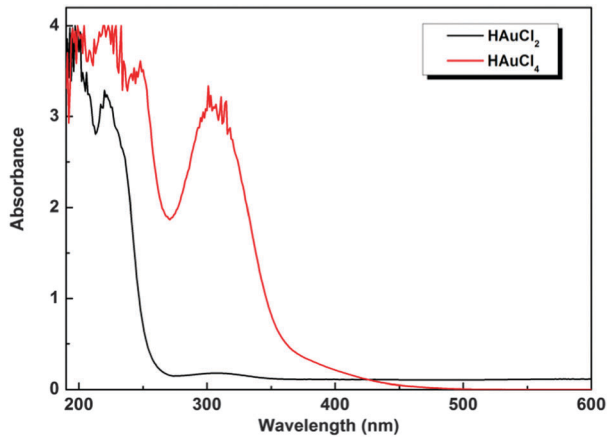

Fig. 1 UV-vis spectra of aqueous solutions of $HAuCl_4$ and $HAuCl_2$.

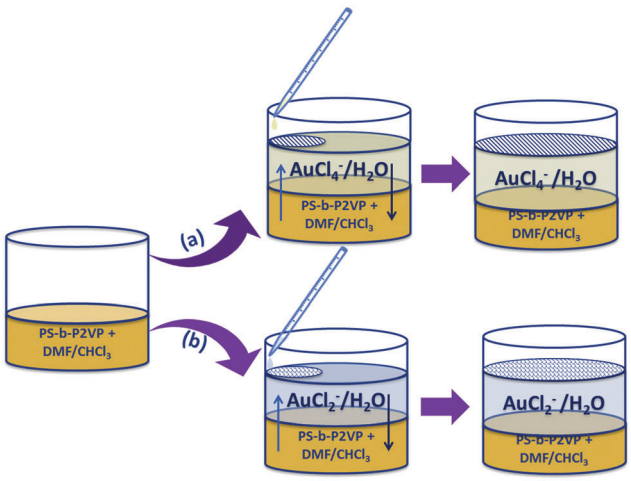

Scheme 1 Schematic representation of the fabrication process of the composite films.

(V_{DMF}/V_{CHCl_3} = 3/2) solution mixed with 0.2 mg mL^{-1} PS-*b*-P2VP was poured into a glass bottle with a diameter of 3.5 cm, after which an equal volume of an aqueous solution of $HAuCl_4$ with a concentration of 0.001 or 0.0005 mol L^{-1} or an aqueous solution of $HAuCl_2$ with a concentration of 0.001 mol L^{-1} was added slowly using a pipette to allow it to run down the inside wall of the bottle to cover the organic solution, resulting in the formation of a clear liquid/liquid interface. The bottle was placed in a sealed container and stored in a dark place. After allowing it to stand for 3 hours, the thin composite film that appeared at the air/liquid interface was deposited onto solid substrates for further characterization.

General characterization

The morphology and structure of the thin films were investigated using high-resolution transmission electron microscopy (HRTEM, JEOL-2010) with an accelerating voltage of 200 kV. The samples were prepared by depositing the thin films on carbon-coated 400 mesh copper grids and drying under ambient conditions. The compositions of these samples were investigated using X-ray photoelectron spectroscopy (XPS, ESCALAB MKII) with a Mg Kα excitation source under a pressure of 1.0×10^{-6} Pa at a resolution of 1.00 eV. UV-vis spectra were obtained using a UV-vis spectrophotometer (HP 8453E). The samples for XPS and UV-vis spectroscopic investigations were prepared by depositing the thin films that formed at the air/liquid interface onto quartz slides and drying at room temperature.

Dynamic light scattering (DLS) measurements

To observe the process by which the composite film was formed, the upper phase was monitored using the DLS technique with a BI-200SM research goniometer and a laser light scattering system (Brookhaven Instruments Corporation). Measurements were carried out at a scattering angle of 90° at room temperature.

Theoretical calculations

All the complexes were fully optimized and characterized with the Gaussian 09 program package[47] using a reliable quantum chemistry method (B3LYP). The aug-cc-pVDZ basis set[48,49] was used for Au, whereas the 6-311++G** basis set was adopted for N, H, C, and Cl atoms. We corrected the interaction energies for the basis set superposition error (BSSE) using the Boys–Bernardi counterpoise scheme.[50]

Catalytic reaction

About 0.5 mL of an aqueous solution of 4-NA with a concentration of 2×10^{-4} mol L^{-1} was poured into a 1 cm quartz cuvette, after which 1.0 mL of an aqueous solution of KBH_4 with a concentration of 2×10^{-2} mol L^{-1} was added. To reduce the Au(III) or Au(I) species completely, the entire composite thin film deposited on quartz slides was treated with the aqueous solution of KBH_4. The treated composite thin film was then immersed in the reaction system to catalyze the reduction of 4-NA to *p*-phenylenediamine. The progress of the reaction was monitored using a UV–vis spectrophotometer (HP 8453E).

Results and discussion

Morphology and structure

Fig. 2 shows photographs of the composite thin films that were fabricated at the air/liquid interface through routes (a) and (b) described in Scheme 1. When the upper phase consisted of the aqueous solution of $AuCl_4^-$ with a concentration of

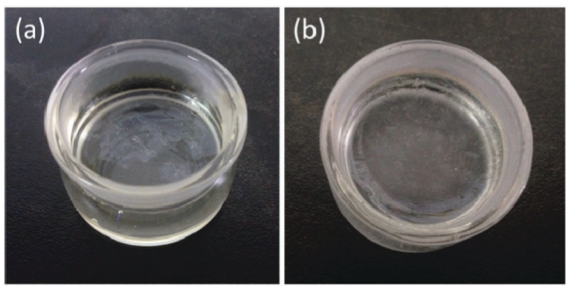

Fig. 2 Photographs of the composite thin films that were fabricated at the air/liquid interface using the $AuCl_4^-$ (a) and $AuCl_2^-$ (b) solutions.

Published on 07 December 2015. Downloaded by Michigan State University on 22/01/2016 03:37:24.

0.001 mol L^{-1}, the formed composite thin film was slightly fragile and scattered over the surface. In contrast, when the aqueous solution of $AuCl_2^-$ was used as the upper phase, a stable, sticky film was obtained across the whole air/liquid interface.

These films were deposited on copper grids and investigated using TEM. As soon as the liquid/liquid interface was formed, the film immediately appeared at the air/water interface. The morphology of the film is mainly nanowire arrays (Fig. 3a and b), whereas a small area of the thin film is covered by sheets of planar films (Fig. 3c). Nanowires with a diameter of about 72 nm were aligned in a parallel fashion and equally spaced, as shown in Fig. 3b. Shortly after the film appeared at the air/liquid interface, the aqueous phase was monitored using dynamic light scattering (DLS) measurements. As shown in Fig. 3d, it was found that particles of a dispersed phase with a size of about 300 nm were formed. When the concentration of the $HAuCl_4$ solution was decreased to 5×10^{-4} mol L^{-1}, a thin, flat film doped with Au nanoclusters appeared at the air/liquid interface (Fig. 3e and f).

The DLS results indicated the formation of molecular assemblies in the aqueous phase. To confirm this, a sample of the aqueous solution was dropped onto a carbon-coated copper grid and absorbed rapidly using a blotting paper. The sample was investigated using TEM, as shown in Fig. S1 (ESI†). Rod-like aggregates, with lengths of several hundreds of nanometers and diameters of 70–80 nm (Fig. S1a, ESI†), and sheet-like aggregates (Fig. S1b, ESI†) appeared, which indicated the formation of cylindrical and disk-like micelles of PS-*b*-P2VP in the mixed solution of water–DMF. The particles on the sheets should be attributed to the reduction of $AuCl_4^-$ ions by copper when the drop was deposited on the copper grid. The nanowire arrays and sheet films shown in Fig. 3a and c should be related to these micelles, respectively.

However, when an aqueous solution of $HAuCl_2$ with the same concentration was used instead, PS-*b*-P2VP self-assembled into a foam structure at the air/liquid interface. As shown in Fig. 4a and b, in this case, the film is composed of microcapsules that are several hundreds of nanometers in size. In addition, the film fabricated in the presence of $HAuCl_2$ is free-standing. The upper phase was also monitored using DLS. The result reveals that aggregates with a mean size of 600 nm were formed. The TEM investigation of the aqueous solution suggests that these aggregates are microcapsules (Fig. S1c, ESI†). It is evident that the foam structure should be related to the microcapsules.

Composition analysis

To analyze the composition of the formed microstructures, the film was additionally studied using XPS. Fig. 5 shows typical XPS spectra of the samples that were formed by PS-*b*-P2VP with 0.001 M $HAuCl_4$ and $HAuCl_2$ solutions. If there was only one species of gold, two symmetrical peaks corresponding to Au $4f_{7/2}$ and $4f_{5/2}$ would have appeared, but the profile of the

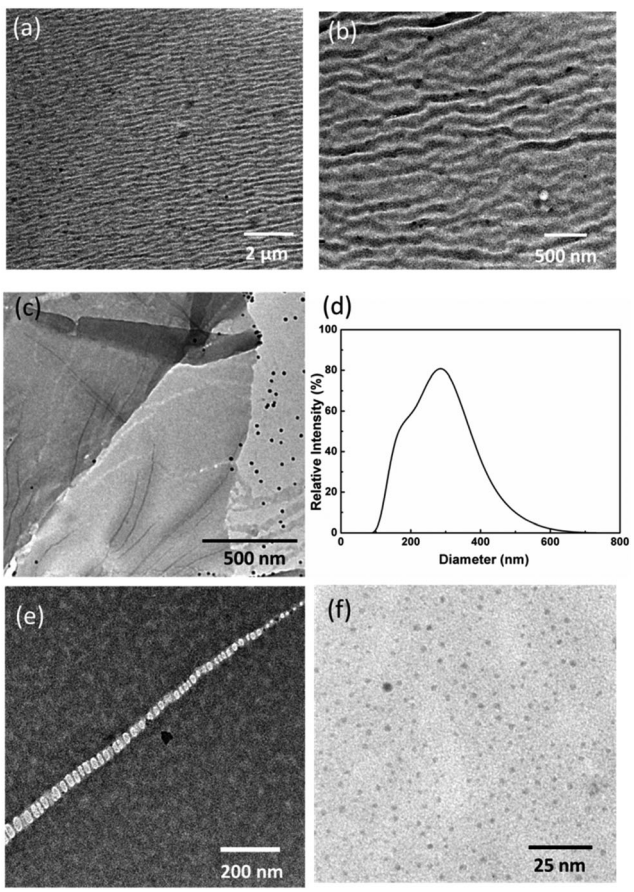

Fig. 3 TEM micrographs of the composite thin films formed at the air/liquid interface with concentrations of $HAuCl_4$ of 0.001 mol L^{-1} (a–c) and 0.0005 mol L^{-1} (e and f) and the DLS spectrum of the upper phase recorded after the film appeared at the air/liquid interface (d).

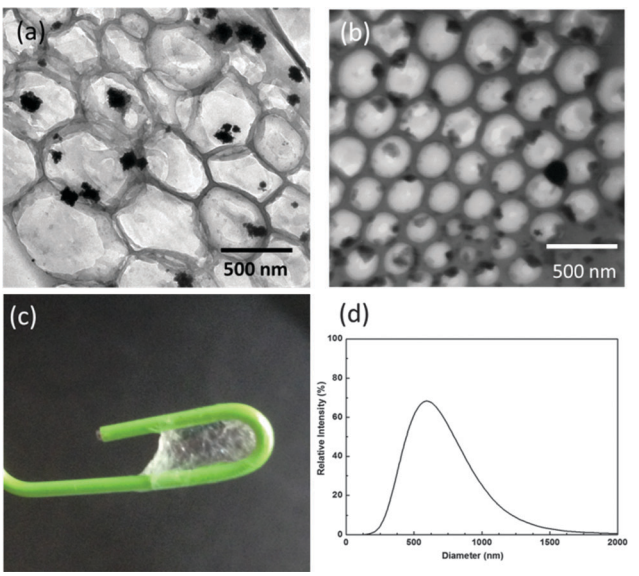

Fig. 4 TEM micrographs of composite thin films formed at the air/liquid interface at a $HAuCl_2$ concentration of 0.001 mol L^{-1} (a and b), a photograph of composite thin film adhered to a clip (c), and DLS results of the upper phase (aqueous solution) observed after 3 h (d).

 This journal is © the Owner Societies 2016

Published on 07 December 2015. Downloaded by Michigan State University on 22/01/2016 03:37:24.

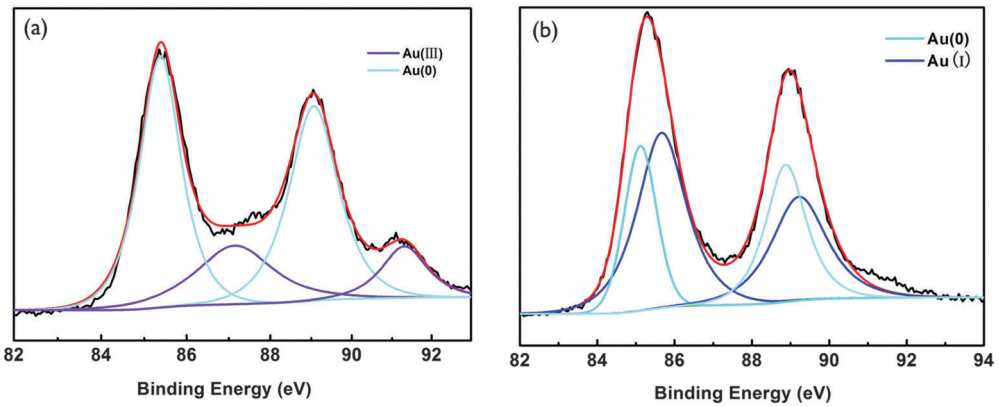

Fig. 5 XPS spectra of thin films of PS-*b*-P2VP/$AuCl_4^-$ (a) and PS-*b*-P2VP/$AuCl_2^-$ (b) formed at the air/liquid interface.

spectrum implies the presence of more than one gold species in the composite film. These bands were deconvoluted into two pairs of peaks located at 85.38/89.06 and 87.14/91.31 eV, respectively, using a Lorentzian multi-peak fitting method, as shown in Fig. 5a. The first pair of peaks was assigned to Au(0) $4f_{7/2}$ and $4f_{5/2}$ spin–orbit coupling. It can be seen that the binding energy of 85.38 eV is much greater than that of bulk Au(0),[51,52] as a result of the formation of gold nanoclusters in the composite film. The second pair of peaks was assigned to Au $4f_{7/2}$ and $4f_{5/2}$ of Au(III),[53,54] which means that two types of gold species, namely, Au(0) and Au(III), coexist in the film. As shown in Fig. 5b, the spectrum was deconvoluted into two pairs of peaks located at 85.11/88.86 eV and 85.66/89.23 eV, which were assigned to $4f_{2/7}$ and $4f_{2/5}$ of Au(0) nanoclusters and Au(I), respectively.[52,55] There was no sign of Au(III) in the XPS spectrum shown in Fig. 5b, suggesting that $AuCl_2^-$, rather than $AuCl_4^-$, played an important role in the fabrication of the film with a foam structure, which additionally indicated that the reduction of $AuCl_4^-$ to $AuCl_2^-$ was complete.

Theoretical calculations

The main driving force behind the formation of both aggregates (PS-*b*-P2VP/$AuCl_4^-$ and PS-*b*-P2VP/$AuCl_2^-$) is hydrophobic interaction. However, electrostatic interaction between the anion ($AuCl_4^-$ and $AuCl_2^-$) and the pyridyl groups may exert a crucial influence on the self-assembly of the polymer molecules. Therefore, the interaction energies were calculated. Theoretical calculations were performed to calculate the counterpoise-corrected interaction energies between the two units in the corresponding fragment. It is worth mentioning that the two complex ions, $AuCl_4^-$ and $AuCl_2^-$, have different geometrical structures, namely, square planar and linear shapes, respectively, as shown in Fig. 6. In addition, the plane of the square planar $AuCl_4^-$ ion is arranged perpendicularly to the plane of the pyridyl group (Fig. 6a), whereas the linear $AuCl_2^-$ molecule is coplanar with the pyridyl group (Fig. 6b). The electrostatic interaction energies between the anions $AuCl_4^-$ and $AuCl_2^-$ and the pyridyl groups were calculated to be −78.26 and −84.07 kJ mol^{-1}, respectively, suggesting that $AuCl_2^-$ formed more stable complexes with protonated pyridyl groups than $AuCl_4^-$.

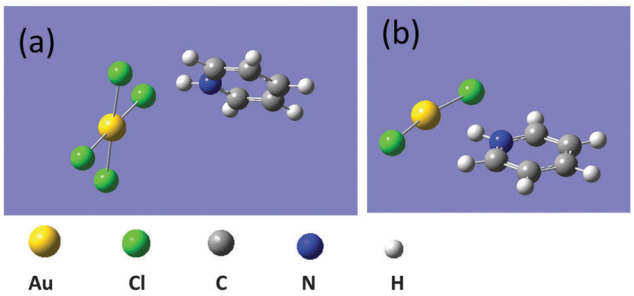

Fig. 6 Optimized geometries of the $AuCl_4^-$/PVP (a) and $AuCl_2^-$/PVP (b) complexes.

Formation mechanism

The abovementioned results enabled us to propose a possible formation mechanism, shown in Scheme 2, by which the nanowire arrays and foam structure were formed at the air/liquid interface using $HAuCl_4$ and $HAuCl_2$ aqueous solutions with the same concentration, respectively. When droplets of DMF with PS-*b*-P2VP and a small amount of $CHCl_3$ were transferred into the aqueous solution, an O/W emulsion was formed as a result of the "ouzo effect". Polymer molecules

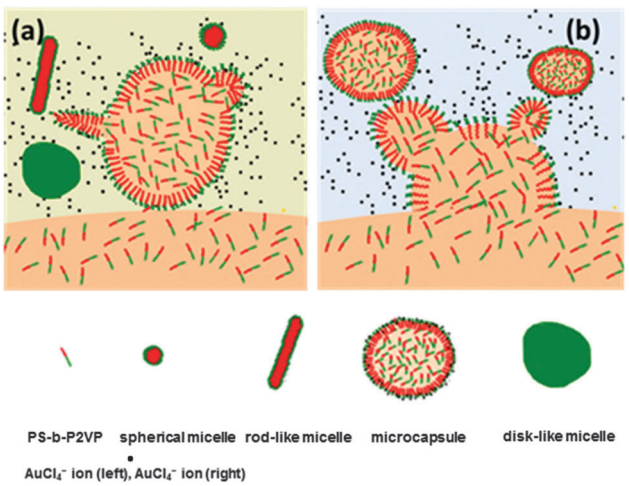

Scheme 2 Formation mechanism of organized polymer assemblies.

Published on 07 December 2015. Downloaded by Michigan State University on 22/01/2016 03:37:24.

formed a tight monolayer around the droplets through adsorption; thus, the droplets can be considered as "solid" particles that tend to be adsorbed at the air/liquid interface to reduce the surface energy. At the same time, DMF molecules have a tendency to diffuse into water due to the miscibility of DMF and water, resulting in the formation of organized molecular assemblies. In fact, the tendency of DMF to diffuse into water and that of the "solid" particles to be adsorbed at the air/liquid interface compete with each other. If DMF molecules are able to easily and rapidly permeate through the tight monolayer into water, the polymer molecules in a mixed medium of water/DMF will self-assemble into aggregates such as cylindrical micelles and flexible sheets, as shown in Scheme 2(a). The particles with a mean size of 300 nm, which was obtained from the DLS observations, should be the formed cylindrical micelles. This was further confirmed by TEM investigations (Fig. S1, ESI†). Subsequently, these aggregates are adsorbed at the air/liquid interface and further self-assemble into micro and nanostructures. On the other hand, if conditions are such that DMF molecules are unable to easily diffuse into water, the microcapsules with a mean size of 600 nm, as is indicated by the DLS observations and TEM investigations (Fig. S1, ESI†), are sufficiently stable, as illustrated in Scheme 2(b), and will be adsorbed at the air/liquid interface, leading to the formation of a foam structure.

It is obvious that the formation of the foam structure in the film follows from the adsorption and accumulation of the microcapsules at the air/liquid interface. Then, the cylindrical micelles are transformed into nanowires at the air/liquid interface. As is well known, the surface tension decreases with the adsorption of surfactants or solid particles at the interface, resulting in the generation and increase of surface pressure. Because the surface layer is very thin, the generated three-dimensional pressure is very high. In fact, this higher pressure has been widely utilized to fabricate nanorods and nanowires with parallel alignment at the air/water interface using the Langmuir monolayer technique such as $BaCrO_4$ nanorods,[56] Ag nanowires,[57] Ge nanowires,[58] carbon nanotubes,[59] and ZnSe nanowires.[60] This pressure has also been used to convert nanorods into nanowires[61] and to transform thin nanowires into thick nanowires[62] at the interface. In this study, the surface pressure generated through Gibbs adsorption was utilized to fabricate the cylindrical micelles with parallel alignment and convert them into nanowire arrays. The process of formation of the nanowire arrays at the air/liquid interface can be described as follows. The cylindrical micelles are oriented randomly at the beginning of the adsorption process. More and more micelles are adsorbed at the interface, leading to a continuous increase in the surface pressure. Thus, these adsorbed micelles are oriented again under the higher surface pressure to form parallel arrays, in which the micelles are connected to each other in an end-to-end fashion. With a further increase in the surface pressure, the connected ends of the micelles are fused, resulting in the formation of the nanowire arrays. This is an interesting application of surface pressure.

Au(III) adopts dsp^2 hybridization to form $AuCl_4^-$, whereas Au(I) adopts sp hybridization to form $AuCl_2^-$ in aqueous solutions. According to theoretical calculations, $AuCl_4^-$ and $AuCl_2^-$ ions exist in square planar and linear shapes, respectively, which means that $AuCl_4^-$ ions may offer larger steric hindrance than $AuCl_2^-$ ions while interacting with the positively charged protonated pyridyl group. In addition, the interaction energies suggest that the complexes that are formed between $AuCl_2^-$ and protonated pyridyl groups are more stable than those that are formed with $AuCl_4^-$, which is consistent with the results of other researchers.[63,64] As a consequence, the adsorption monolayer of PS-*b*-P2VP around the droplets is insufficiently tight when binding to $AuCl_4^-$, allowing the DMF molecules to easily and rapidly permeate through the monolayer, thereby resulting in the formation of micelles. According to the critical packing parameter (p) theory, when $p < 1/3$, spherical micelles are formed; when $1/3 < p < 1/2$, rod-like or cylindrical micelles are formed; when $1/2 < p < 1$, flexible lamellae or vesicles appear; finally, when $p = 1$, planar lamellae are obtained. In the beginning, the stronger interaction between $AuCl_4^-$, with a concentration of 0.001 mol L^{-1}, and the pyridyl group results in p being less than 1/2, which leads to cylindrical micelles. As $AuCl_4^-$ is gradually consumed, the interaction between the pyridyl groups and the $AuCl_4^-$ ions decreases, the P2VP block extends, and the value of p increases to close to 1, which results in the formation of disk-like micelles. This is the reason why a thin, flat film is formed at the air/liquid interface (Fig. 3e and f) when using a $HAuCl_4$ aqueous solution with a concentration of 5×10^{-4} mol L^{-1}. In contrast, the polymer molecules form a much tighter monolayer around the droplets when binding with $AuCl_2^-$, which prevents DMF from easily diffusing into the aqueous solution; thus, the stable microcapsules adsorb and assemble into a foam structure at the air/liquid interface.

It should be noted that the mean diameters of the nanowires were 52 and 72 nm, respectively, when aqueous solutions of 0.01 mol L^{-1} $AgNO_3$ and 0.001 mol L^{-1} $HAuCl_4$ were used.[43] In an Ag^+ system, one silver ion would coordinate to two pyridyl groups in the same polymer chain or adjacent polymer chains, leading to the vertical compression of the P2VP block, whereas in an aqueous solution of $HAuCl_4$, compared with the P2VP/Ag^+ system, the P2VP chain would be expected to expand somewhat because of electrostatic repulsion between the protonated pyridyl groups. Although cylindrical micelles and nanowires were formed in both of these cases, respectively, their diameters are different from each other.

In addition, the influences of the block copolymer concentration, the volume ratio of DMF/$CHCl_3$, and the volume ratio of the organic and aqueous solutions were investigated. These results are described and discussed in the ESI† (Fig. S2–S4).

Catalytic properties

The catalytic properties of the composite films prepared with $HAuCl_4$ and $HAuCl_2$ were investigated by doping with Au nanoclusters. These composites are anticipated to exhibit high catalytic activity for selected heterogeneous catalytic reactions such as the reduction of 4-NA. Fig. 7 exhibits the time-dependent

 This journal is © the Owner Societies 2016

Published on 07 December 2015. Downloaded by Michigan State University on 22/01/2016 03:37:24.

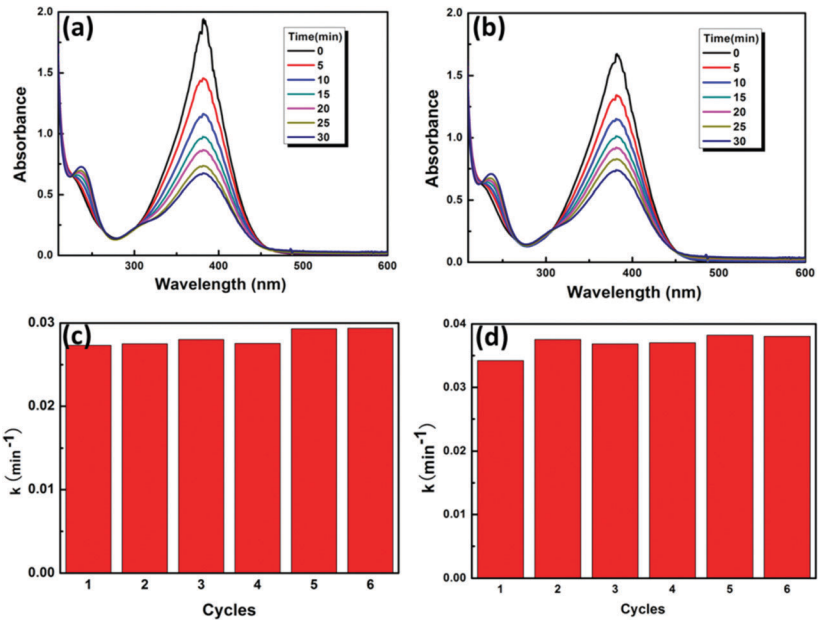

Fig. 7 Catalytic reduction of 4-NA to *p*-phenylenediamine. Typical time-dependent absorption spectra of the reaction solution in the presence of a composite thin film prepared using $HAuCl_4$ (a) and $HAuCl_2$ (b) and reaction rate constants for six successive cycles of reduction using a composite thin film prepared with $HAuCl_4$ (c) and $HAuCl_2$ (d) as the catalyst.

absorption spectra of the reaction solution in the presence of a composite thin film at room temperature. It is clear that the intensity of the peak at 382 nm decreased and a new peak at 237 nm corresponding to *p*-phenylenediamine appeared with time. This is regarded to be a pseudo-first-order reaction. The apparent rate constant was obtained from the slope of the linear-fitted plot of $\ln(A_t/A_0)$ *versus t*. The apparent rate constants obtained when using the composite films as catalysts are shown in Fig. 7. The values of *k* are in close proximity to each other, indicating that the thin films prepared with $HAuCl_4$ and $HAuCl_2$ are both stable and reusable.

Conclusion

In summary, composite thin films doped with Au species were fabricated at the air/liquid interface using a unique and facile approach in which mass transfer across a liquid/liquid interface, self-assembly of block copolymer molecules in an aqueous phase, Gibbs adsorption of formed aggregates such as micelles at the air/liquid interface, and further organization at the interface were combined. The contributions of two different Au species, namely, $AuCl_4^-$ and $AuCl_2^-$, were examined and found to exert a significant influence on the adsorption and self-assembly behavior of the polymers and on the architecture of the final microstructure, namely, nanowire arrays and a foam structure, respectively. In addition, the influences of other experimental conditions on the structures of the films were investigated. Besides, the films doped with Au species were reduced to Au nanoclusters, which exhibited effective catalytic activity in heterogeneous catalytic reactions such as the reduction of nitro compounds in aqueous solutions.

Acknowledgements

This study was supported by grants from the National Natural Science Foundation of China (No. 21273133).

Notes and references

1 B. M. Discher, Y. Y. Won, D. S. Ege, J. C. Lee, F. S. Bates, D. E. Discher and D. A. Hammer, *Science*, 1999, **284**, 1143.
2 L. Zhang and A. Eisenberg, *J. Am. Chem. Soc.*, 1996, **118** 3168.
3 T. Azzam and A. Eisenberg, *Angew. Chem., Int. Ed.*, 2006, **45**, 7443.
4 R. Vyhnalkova, L. Xiao, G. Yang and A. Eisenberg, *Langmuir*, 2014, **30**, 2188.
5 Y. Shi, W. Zhu, D. Yao, M. Long, B. Peng, K. Zhang and Y. Chen, *ACS Macro Lett.*, 2014, **3**, 70.
6 E. Han, K. O. Stuen, M. Leolukman, C.-C. Liu, P. F. Nealey and P. Gopalan, *Macromolecules*, 2009, **42**, 4896.
7 D. U. Ahn and E. Sancaktar, *Soft Matter*, 2008, **4**, 1454.
8 Y. Lu, H. Xia, G. Zhang and C. Wu, *J. Mater. Chem.*, 2009, **19**, 5952.
9 H. Park, J.-U. Kim and S. Park, *Nanoscale*, 2012, **4**, 1362.
10 K. G. Yager, E. Lai and C. T. Black, *ACS Nano*, 2014, **8**, 10582.
11 I. I. Perepichka, A. Badia and C. G. Bazuin, *ACS Nano*, 2010, **4**, 6825.
12 J. K. Cox, K. Yu, B. Constantine, A. Eisenberg and R. B. Lennox, *Langmuir*, 1999, **15**, 7714.
13 E. W. Price, Y. Guo, C. W. Wang and M. G. Moffitt, *Langmuir*, 2009, **25**, 6398.
14 L. Zhao, C. Feng, X. Pang, J. Jung, M. C. Stefan, P. Sista and Z. Lin, *Soft Matter*, 2013, **9**, 8050.

Published on 07 December 2015. Downloaded by Michigan State University on 22/01/2016 03:37:24.

15 J. Y. Park and R. C. Advincula, *Soft Matter*, 2011, **7**, 9829.
16 B. Chung, M. Choi, M. Ree, J. C. Jung, W. C. Zin and T. Chang, *Macromolecules*, 2006, **39**, 684.
17 B. Chung, H. Choi, H.-W. Park, M. Ree, J. C. Jung, W. C. Zin and T. Chang, *Macromolecules*, 2008, **41**, 1760.
18 G. Wen, B. Chung and T. Chang, *Polymer*, 2006, **47**, 8575.
19 G. Wen, *J. Phys. Chem. B*, 2010, **114**, 3827.
20 G. Wen, B. Chung and T. Chang, *Macromol. Rapid Commun.*, 2008, **29**, 1248.
21 Y.-S. Seo, K. S. Kim, A. Galambos, R. G. H. Lammertink, G. J. Vancso, J. Sokolov and M. Rafailovich, *Nano Lett.*, 2004, **4**, 483.
22 H. Lu, B. Akgun, X. Wei, L. Li, S. K. Satija and T. P. Russell, *Langmuir*, 2011, **27**, 12443.
23 S. Yang, C. F. Wang and S. Chen, *J. Am. Chem. Soc.*, 2014, **133**, 8412.
24 L.-J. Chen, H. Ma, K. Chen, H.-R. Cha, Y.-I. Lee, D.-J. Qian and H.-G. Liu, *J. Colloid Interface Sci.*, 2011, **362**, 81.
25 L. Lin, K. Shang, X. Xu, C. Chu, H. Ma, Y.-I. Lee and H.-G. Liu, *J. Phys. Chem. B*, 2011, **115**, 11113.
26 C. Zhou, N. Chen, J. Yang, H. Liu and Y. Li, *Macromol. Rapid Commun.*, 2012, **33**, 688.
27 D. E. Gragson, J. M. Jensen and S. M. Baker, *Langmuir*, 1999, **15**, 6127.
28 J. Juárez, S. Goy-López, A. Cambón, M. A. Valdez, P. Taboada and V. Mosquera, *J. Phys. Chem. C*, 2010, **114**, 15703.
29 Y.-J. Chen, T. Liu, X.-R. Zhai and G.-Y. Xu, *Acta Phys.-Chim. Sin.*, 2014, **30**, 102.
30 A. A. Steinschulte, W. Xu, F. Draber, P. Hebber, A. Jung, D. Bogdanovski, S. Schneider, V. Tsukruk and F. A. Plamper, *Soft Matter*, 2015, **11**, 3559.
31 Z. Sun, T. Feng and T. P. Russell, *Langmuir*, 2013, **29**, 13407.
32 Y. G. He, S. Y. Shi, N. Liu, Y. Y. Zhu, Y. S. Ding, J. Yin and Z. Q. Wu, *RSC Adv.*, 2015, **5**, 39697.
33 B. Du, X. Chen, B. Zhao, A. Mei, Q. Wang, J. Xu and Z. Fan, *Nanoscale*, 2010, **2**, 1684.
34 D. Wang, H. Ma, C. Chu, C. Chu, J. Hao and H.-G. Liu, *J. Colloid Interface Sci.*, 2013, **402**, 75.
35 Y. Liu, L. Chen, Y. Geng, Y.-I. Lee, Y. Li, J. Hao and H.-G. Liu, *J. Colloid Interface Sci.*, 2013, **407**, 225.
36 C. Chu, D. Wang, H. Ma, M. Yu, J. Hao and H.-G. Liu, *Mater. Chem. Phys.*, 2013, **142**, 259.
37 K. Shang, Y. Geng, X. Xu, C. Wang, Y.-I. Lee, J. Hao and H.-G. Liu, *Mater. Chem. Phys.*, 2014, **146**, 88.
38 M. Liu, Y. Geng, K. Tong, J. Xu, Y.-I. Lee, J. Hao and H.-G. Liu, *RSC Adv.*, 2015, **5**, 4334.
39 Y. Geng, M. Liu, K. Tong, J. Xu, Y.-I. Lee, J. Hao and H.-G. Liu, *Langmuir*, 2014, **30**, 2178.
40 M. Liu, Q. Wang, Y. Geng, C. Wang, Y.-I. Lee, J. Hao and H.-G. Liu, *Langmuir*, 2014, **30**, 10503.
41 M. Hong, Y. Geng, M. Liu, Y. Xu, Y.-I. Lee, J. Hao and H.-G. Liu, *J. Colloid Interface Sci.*, 2015, **438**, 212.
42 M. J. Hollamby, D. Borisova, H. Möhwald and D. Shchukin, *Chem. Commun.*, 2012, **48**, 115.
43 X. Zhao, Q. Wang, Y.-I. Lee, J. Hao and H.-G. Liu, *Chem. Commun.*, 2015, **51**, 16687.
44 Q. Wang, X. Zhao, Y.-I. Lee and H.-G. Liu, *RSC Adv.*, 2015, **5**, 86564.
45 C. J. Johnson, E. Dujardin, S. A. Davis, C. J. Murphy and S. Mann, *J. Mater. Chem.*, 2002, **12**, 1765.
46 J. Perez-Juste, L. M. Liz-Marzan, S. Carnie, D. Y. Chan and P. Mulvaney, *Adv. Funct. Mater.*, 2004, **14**, 571.
47 M. J. Frisch, G. W. Trucks, H. B. Schlegel, G. E. Scuseria, M. A. Robb, J. R. Cheeseman, G. Scalmani, V. Barone, B. Mennucci, G. A. Petersson, H. Nakatsuji, M. Caricato, X. Li, H. P. Hratchian, A. F. Izmaylov, J. Bloino, G. Zheng, J. L. Sonnenberg, M. Hada, M. Ehara, K. Toyota, R. Fukuda, J. Hasegawa, M. Ishida, T. Nakajima, Y. Honda, O. Kitao, H. Nakai, T. Vreven, J. A. Montgomery, J. E. Peralta, F. Ogliaro, M. Bearpark, J. J. Heyd, E. Brothers, K. N. Kudin, V. N. Staroverov, R. Kobayashi, J. Normand, K. Raghavachari, A. Rendell, J. C. Burant, S. S. Iyengar, J. Tomasi, M. Cossi, N. Rega, J. M. Millam, M. Klene, J. E. Knox, J. B. Cross, V. Bakken, C. Adamo, J. Jaramillo, R. Gomperts, R. E. Stratmann, O. Yazyev, A. J. Austin, R. Cammi, C. Pomelli, J. W. Ochterski, R. L. Martin, K. Morokuma, V. G. Zakrzewski, G. A. Voth, P. Salvador, J. J. Dannenberg, S. Dapprich, A. D. Daniels, Ö. Farkas, J. B. Foresman, J. V. Ortiz, J. Cioslowski and D. J. Fox, *Gaussian 09, revision A.1*, Gaussian, Inc., Wallingford, CT, 2009.
48 D. Figgen, G. Rauhut, M. Dolg and H. Stoll, *Chem. Phys.*, 2005, **3**, 227.
49 K. A. Peterson and C. Puzzarini, *Theor. Chem. Acc.*, 2005, **114**, 283.
50 S. F. Boys and F. Bernardi, *Mol. Phys.*, 1970, **19**, 553.
51 K. Kishi and S. Ikeda, *J. Phys. Chem.*, 1974, **78**, 107.
52 J. R. Mycroft, G. M Bancroft, N. S. McIntyre and J. W. Lorimer, *Geochim. Cosmochim. Acta*, 1995, **59**, 3351.
53 J.-P. Sylvestre, S. Poulin, A. V. Kabashin, E. Sacher, M. Meunier and J. H. Luong, *J. Phys. Chem. B*, 2004, **108**, 16864.
54 H. Muto, K. Yamada, K. Miyajima and F. Mafune, *J. Phys. Chem. C*, 2007, **111**, 17221.
55 H.-L. Zhang, S. D. Evans, J. R. Henderson, R. E. Miles and T. Shen, *J. Phys. Chem. B*, 2003, **107**, 6087.
56 F. Kim, S. Kwan, J. Akana and P. Yang, *J. Am. Chem. Soc.*, 2001, **123**, 4360.
57 A. Tao, F. Kim, C. Hess, J. Goldberger, R. He, Y. Sun, Y. Xia and P. Yang, *Nano Lett.*, 2003, **3**, 1229.
58 D. Wang, Y.-L. Chang, Z. Liu and H. Dai, *J. Am. Chem. Soc.*, 2005, **127**, 11871.
59 X. Li, L. Zhang, X. Wang, I. Shimoyama, X. Sun, W.-S. Seo and H. Dai, *J. Am. Chem. Soc.*, 2007, **129**, 4890.
60 S. Acharya, A. B. Panda, N. Belman, S. Efrima and Y. Golan, *Adv. Mater.*, 2006, **18**, 210.
61 S. Acharya and S. Efrima, *J. Am. Chem. Soc.*, 2005, **127**, 3486.
62 I. Patla, S. Acharya, L. Zeiri, J. Israelachvili, S. Efrima and Y. Golan, *Nano Lett.*, 2007, **7**, 1459.
63 J. Pérez-Juste, L. M. Liz-Marzán, S. Carnie, D. Y. C. Chan and P. Mulvaney, *Adv. Funct. Mater.*, 2004, **14**, 571.
64 W. Wang, Y. Han, M. Tian, Y. Fan, Y. Tang, M. Gao and Y. Wang, *ACS Appl. Mater. Interfaces*, 2013, **5**, 5709.

 This journal is © the Owner Societies 2016